This paper describes objective technical results and analysis. Any subjective views or opinions that might be expressed in the paper do not necessarily represent the views of the U.S. Department of Energy or the United States Government.

SAND2019-6728J

Effects of Nitrogen on the Interface Density of States Distribution in 4H-SiC Metal Oxide Semiconductor Field Effect Transistors: Super-hyperfine Interactions and Near Interface Silicon Vacancy Energy Levels

Mark A. Anders, National Institute of Standards and Technology (NIST), 100 Bureau Drive, Gaithersburg, MD 20899

Patrick M. Lenahan, Department of Engineering Science and Mechanics, 212 EES Bldg. Pennsylvania State University, University Park, PA 16802

Arthur H. Edwards, Space Vehicles Directorate, Air Force Research Laboratory, Kirtland Air Force Base, New Mexico, 87117-5776

Peter A. Schultz, Sandia National Laboratories, Albuquerque, NM 87185-1322 USA

Renee M. Van Ginhoven, Directed Energy Directorate, Air Force Research Laboratory, Kirtland Air Force Base, New Mexico, 87117-5776

Abstract

The performance of SiC-based metal-oxide-semiconductor field-effect transistors (MOSFETs) is greatly enhanced by a post oxidation anneal in NO. These anneals greatly improve effective channel mobilities and substantially decrease interface trap densities. In this work, we investigate the effect of NO anneals on the interface density of states though density functional theory (DFT) calculations and electrically detected magnetic resonance (EDMR) measurements. EDMR measurements on 4H-SiC MOSFETs indicate that NO annealing substantially reduces the density of near interface SiC silicon vacancy centers: it results in a thirty-fold reduction in the EDMR amplitude. The anneal also alters post NO anneal resonance line shapes significantly. EDMR measurements exclusively sensitive to interface traps with near mid-gap energy levels have line shapes relatively unaffected by NO anneals whereas measurements sensitive to defects with energy levels more broadly distributed in the 4H-SiC band gap are significantly altered by the anneals. We show that the observed change in EDMR linewidth and the correlation with energy levels can be explained by nitrogen atoms introduced by the NO annealing substituting into nearby carbon sites of silicon vacancy defects.

Introduction

Metal-oxide-semiconductor field-effect transistors (MOSFETs) based on silicon dioxide (SiO_2) on 4H-silicon carbide (4H-SiC) show great promise in high power and high temperature applications. However, the potential of this technology is limited by less than ideal electronic behavior at the SiC/SiO_2 interface region. Incorporation of post-oxidation NO annealing into the process flow results in significant densities of nitrogen in the interfacial region [1,2] along with substantial improvement of the interface properties-- typically an order of magnitude improvement in effective channel mobility [3] and a comparable decrease in interface trap density [4-6]. Although

Sandia National Laboratories is a multimission laboratory managed and operated by National Technology & Engineering Solutions of Sandia, LLC, a wholly owned subsidiary of Honeywell International Inc., for the U.S. Department of Energy's National Nuclear Security Administration under contract DE-NA0003525.

the NO anneals are of great technological importance in SiC MOSFET technology, the materials physics involved in the annealing process is not well understood. Important physical insight can be gathered from electron paramagnetic resonance (EPR) measurements [7] obtained via electrically detected magnetic resonance (EDMR) [8, 9]. EDMR studies show that NO anneals result in substantial reduction in the magnetic resonance spectrum associated with silicon vacancy (V_{Si}) centers located near the SiC/SiO_2 interface [10], as indicated in Fig. 1. [1]

Two different EDMR techniques, spin dependent recombination (SDR) [2] and spin dependent charge pumping (SDCP) [12], offer complementary information about the energy levels of the observed defects. The SDR approach is specifically sensitive to defects with energy levels near mid-gap while SDCP is sensitive to defect levels throughout most (about 85% in our case) of the band gap (centered roughly at mid-gap). The line shape of the (dramatically reduced) post-anneal EDMR spectrum depends on the EDMR detection technique. If the EDMR is detected via SDR, the post-anneal device spectrum is virtually identical to the as-grown device spectrum. However, if the EDMR is detected via SDCP, the post-anneal spectrum is much broader than the as-grown device spectrum. Additionally, for measurements taken prior to any anneal, the spectral linewidths are virtually identical for SDR and SDCP, but for the post-annealed MOSFET's, the spectra are significantly different; the SDCP spectrum is much broader than the SDR spectrum. This difference is clear in both high and ultra-low resonant frequency EDMR measurements. However, the differences are most evident in the ultra-low frequency spectra. Representative results are illustrated in Figs. 2 and 3 which compare ultra-low frequency measurements of NO annealed and as-grown MOSFETs via both EDMR techniques.

In the current work, we use density functional theory (DFT) to show that the NO anneal-induced broadening of the EDMR response in ultra-low field and frequency SDCP measurements, about 1.5 Gauss, is consistent with hyperfine interactions from nitrogen atoms introduced as third-nearest neighbors to paramagnetic silicon vacancies.[2] Candidate nitrogen sites are shown in Fig. 4. We show that the presence of nitrogen atoms at those third nearest neighbor sites substantially lower the energy level associated with the EDMR resonance, the –/0 level, by approximately 0.5 eV; this result provides an explanation for the difference between the SDR and SDCP measurements.

To provide a coherent discussion of our analysis, we first give a brief discussion of EPR and EDMR in general, and then we describe the SDR and SDCP EDMR detection techniques. EPR occurs when a paramagnetic center in a magnetic field absorbs electromagnetic radiation at a frequency ν. In the simplest case of an unpaired electron unperturbed by its environment, the electron transitions from its ½ to -½ spin state (or vice versa) with a resonance condition given by [7]:

$$h\nu = g_e \mu_B B. \quad (1)$$

---

[1] The EDMR results also show a large reduction of a second spectrum consisting of two lines with a separation of approximately 11 Gauss. This spectrum is attributed to a hydrogen complexed oxygen deficient silicon site called the 10.4 doublet center [11]. This aspect of the EDMR will not be further discussed in this work.

[2] The silicon vacancy is surrounded by four carbon nearest neighbors, twelve silicon second-nearest neighbors (in two distinct shells), and 25 carbon third-nearest neighbors (in six distinct shells).

Here, h is Planck's constant, ν is the electromagnetic radiation frequency, g_e is the free electron g factor (g_e= 2.0023193…), μ_B is the Bohr magneton, and B is an externally applied magnetic field.

The analytical power of EPR (and EDMR) comes from deviations from this simple case caused by the paramagnetic site environment. For the observations in this study, two phenomena dominate these deviations: spin-orbit coupling and electron-nuclear hyperfine interactions. For the purpose of our discussion, the spin Hamiltonian of such a system can be expressed as [7]:

$$\mathcal{H} = \mu_B \boldsymbol{B} \cdot \boldsymbol{g} \cdot \mathbf{S} + \sum_i \mathbf{I}_i \cdot \boldsymbol{A_i} \cdot \mathbf{S}. \tag{2}$$

Here, μ_B is the Bohr magneton, $\boldsymbol{B}$ is the applied magnetic field vector, $\mathbf{S}$ is the electronic spin operator, and $\mathbf{I}_i$ is the nuclear spin operator for the ith nucleus. $\boldsymbol{g}$ and $\boldsymbol{A_i}$ are essentially tensors which describe a defect's local environment and are usually referred to as the g and A tensors. Spin-orbit coupling causes the g tensor components to deviate from the free electron g_e, and A provides a measure of electron-nuclear hyperfine interactions. It should be noted that a more complex spin Hamiltonian is required to fully describe the silicon vacancies discussed herein. However, the simple form of equation (2) is adequate to understand the results presented in this work.

EDMR measurements detect EPR through a change in device current. As such, EDMR is inherently advantageous for solid state electronic device studies for two reasons: (1) it is exclusively sensitive to defects involved in electronic transport and (2) it is typically at least ten million times more sensitive than conventional EPR. In an EDMR measurement of an electronic device, the device is placed into a high quality factor microwave cavity or an RF coil which is placed in an electromagnet. As is the case for conventional EPR, the device is exposed to constant frequency electromagnetic radiation. Unlike conventional EPR, in EDMR, the device under study is biased in such a way as to produce a recombination or trap assisted tunneling dominated current. The magnetic field is slowly and linearly swept about the resonance field, and the EPR-induced current change is measured as a function of the magnetic field. The EDMR measurements discussed in this paper are, as mentioned previously, SDR and SDCP.

SDR occurs when a charge carrier in either the valence or conduction band transitions to a deep level defect, and then recombines through the subsequent capture of a charge carrier of the opposite sign. This process is spin dependent. A somewhat simplified explanation, suitable for the discussion herein, is as follows. The process is spin dependent because the capture event involving a paramagnetic charge carrier (electron or hole) at a paramagnetic defect site can only take place when the two entities have opposite spins. Envision the simple case of a conduction electron encountering a neutral paramagnetic "dangling bond" site. If the conduction electron and dangling bond electrons have the same spin quantum number, the capture event would be forbidden by the Pauli exclusion principle. However, if the dangling bond spin were to be "flipped" by an EPR event, the trapping process and eventual recombination would be allowed. Inducing EPR of defect sites thus increases the recombination rate and recombination current.

One may greatly increase sensitivity to defects at the SiC/SiO_2 interface by utilizing the bipolar amplification effect (BAE) technique [13], which uses SDR, to detect EPR in a lateral channel current. For this reason, our measurements utilize this technique. In the BAE measurement, the MOSFET source-body diode is forward biased. The gate is biased as to attract the charge carriers injected by the source; however, the bias is not sufficient to create an inversion layer. Current is measured at the drain (the drain is at virtual ground), and is strongly influenced by interface/near interface recombination events. The BAE response is optimized by selecting a gate voltage that maximizes the change in interface/near interface recombination current. This change in recombination current as a function of magnetic field is the BAE signal. As is the case with SDR, the BAE technique is only sensitive to deep levels, as they must be efficient recombination centers.

SDCP measurements utilize EPR to observe change in the current produced by charge pumping (CP) [14-16]. SDCP, like SDR, exploits the spin dependent nature of charge capture. Unlike SDR, however, SDCP can be sensitive to defect levels throughout a large majority of the 4H-SiC band gap. SDCP utilizes CP, a powerful and widely utilized electrical MOSFET interface trap characterization technique. The CP process, in the most straightforward approach, involves application of a continuous trapezoidal waveform to the MOSFET gate to alternately invert and accumulate the interface, filling and emptying traps at the interface region. The process produces a recombination current dominated by interface traps called the CP current which is measured at the body contact. Thus, the SDCP response (ΔI_{CP}) is the EPR-induced change in CP current. For our discussion, the most relevant aspect of the technique is its ability to directly connect EDMR spectra with a range of energy levels within the 4H-SiC bandgap. The CP current is proportional to the waveform frequency, charge, effective channel area, density of states, and the measured band gap energy window (ΔE_{CP}). ΔE_{CP} is nearly centered around mid-gap and can be approximated by [14-16]:

$$\Delta E_{CP} = 2k_B T \ln\left(\frac{\Delta V_G}{\overline{v_{th}}\,\overline{\sigma}\,n_i\,(V_{TH}^{CP} - V_{FB}^{CP})\sqrt{t_r t_f}}\right), \tag{3}$$

where, k_B is Boltzmann's constant, T is temperature, ΔV_G is the gate waveform pulse amplitude, $\overline{v_{th}}$ is the geometric average of the electron and hole thermal velocity, $\overline{\sigma}$ is the geometric average of the electron and hole capture cross sections, n_i is the intrinsic carrier concentration, V_{TH}^{CP} and V_{FB}^{CP} are the CP threshold and flatband voltages, respectively, and t_r and t_f are the rise and fall times of the gate waveform, respectively. Equation (3) directly links measured defects to the range of energy levels at which they reside, thus providing a direct link between defect structure and an energy window.

Experimental

Electrically Detected Magnetic Resonance

Our SDCP and BAE measurements were made on a homemade EDMR spectrometer operating at ultra-low frequency (ν = 360 MHz). It consists of a custom-made electromagnet made of 5 nested pairs of Helmholtz coils, a Kepco BOP 100-4M power supply, a Lake Shore Cryotronics 450 DSP temperature-compensated Gauss meter and Hall probe, a Stanford Research Instruments SG382

microwave generator, and a computer which provides lock-in detection, magnetic field control, and the data acquisition system. The RF magnetic field is provided by a Doty Scientific surface coil and resonance circuit. The RLC circuits maximize the RF fields at 360 MHz. Because the spectrometer utilizes lock-in detection, a small audio frequency alternating magnetic field is added to the large swept magnetic field to modulate resonance. As a consequence of this detection method, the measured spectrum is approximately the derivative of the EDMR response. For SDCP measurements, the gate waveform was applied with a Tabor Electronics WW2572A waveform generator. All measurements were made at room temperature.

Two types of MOSFETs were utilized in this study. Both types have a wet thermal gate oxide process, but were fabricated by different manufacturers. One type received a post-oxidation anneal in NO for 2 hours at 1175 °C while the other did not. The NO annealed and as-grown MOSFETs had a doping density, mobility, and defect density of 7 x 10^{16} cm^{-3}, 19 cm^2/Vs, 4.6 x 10^{11} cm^{-2} eV^{-1} and 7 x 10^{16} cm^{-3}, 1 cm^2/Vs, 3.1 x 10^{12} cm^{-2} eV^{-1}, respectively. BAE measurements utilized longer channel MOSFETs which had gate areas (L x W) of 5 x 100 μm^2 (as-grown) and 100 x 100 μm^2 (NO anneal), and SDCP utilized shorter channel MOSFETs which had gate areas (L x W) of 1 x 424 μm2 (as-grown) and 1 x 1000 μm2 (NO anneal).

Theory

The defect calculations were executed with the highly efficient SEQQUEST DFT code, using well converged, local orbital bases (double-zeta + polarization) and Hamann-type pseudopotentials [17], with a spin-polarized Perdew-Becke-Ernzerhoff (PBE) implementation of the generalized gradient approximation [18]. To incorporate self-consistently the correct asymptotic boundary conditions for isolated charged defects, we use the local moment counter charge (LMCC) method [19,20] instead of a *jellium* background charge. This technique has predicted defect level energies with 0.1-0.2 eV accuracy across a full band gap in silicon [21,22], gallium arsenide [23, 24], and cesium iodide [25]. The long-range dielectric screening energy (outside the DFT defect simulation cell) is incorporated using a Jost expression [26] for a charge Q in spherical cavity in isotropic dielectric medium with low frequency dielectric constant, ϵ_o,:

$$E_{pol} = -\frac{Q^2}{2R_{Jost}}\left[1 - \frac{1}{\epsilon_o}\right] \quad (4)$$

where R_{Jost} is an effective "spherical radius" of the supercell (Rydberg atomic units). Good convergence to an asymptotic limit as a function of supercell size verifies that this is a good approximation [23].

We use 2H-SiC as a proxy for 4H. It offers more convenient supercell dimensions, and 2H and 4H defect levels are very similar [27]. We use a 300-atom supercell (a 5x5x3 expansion of the conventional 4-atom hexagonal unit cell) with a 2x2x2 k-sampling. Using our PBE lattice parameters, c = 5.09 Å and a = 3.10 Å, this 5x5x3 supercell has a c/a ratio of 0.985, convenient for applying the spherical Jost screening estimate. We considered nitrogen substitutions depicted in Fig. 4: several substitutions on nearby carbon sites. We also considered two cases where

nitrogen replaced second nearest neighbor silicon. These were found to be significantly (~7eV) higher in energy and therefore not considered further in this work. We considered low- and high-spin configurations. In all cases the high-spin state was lower in energy by roughly 0.2-0.3 eV.

Theoretical Results

In Table I, we show the energies of formation, ΔE_f, in the neutral charge state (in a Si-rich limit), and $R_{N-V_{Si}}$ for the various N-V_{Si} configurations. The stability of nitrogen at carbon sites, N_C, changes remarkably little with distance from the vacancy. Assuming equilibrium conditions, there would be half as many N_C substitutions at 4.78 Å, and 0.003 as many at 5.87 Å, as there are at 3.36 Å.

In Fig. 5, we show computed defect levels for isolated V_{Si}, and for the nitrogen substituting for carbon atoms near a V_{Si}. We label the levels for the N_C sites with the analogous charge state of the isolated silicon vacancy. We expect that the N_C will donate one of its electrons to the V_{Si}, so that the neutral $V_{Si} + N_C$ defect complex corresponds to *-1* charge state of the vacancy and a positive nitrogen defect. This simple picture is supported by the preservation of the general features of the V_{Si} level diagram, with shifts downward, consistent with the N_C acting as a modest perturbation on the V_{Si}. The further the nitrogen ion is from the V_{Si}, the smaller the shift. The –/0 level is relevant to the EDMR results. The largest shift of this level, for the nearest nitrogen, N-a, is ~ 0.5 eV. Note that Fig. 5 has no reference to the band edges. In Fig. 6, we compare our defects levels for the V_{Si} from several calculations in literature [27-29]. Note that only the results from Ref. [28], by Zyweitz and coworkers, and the current work put the –/0 level near mid-gap. However, results in Ref. [28] did not account for finite cell effects. Finally, the band edges in Fig. 6 imply that the +/++ level will be subsumed into the valence band.

The downward shift in the near-midgap –/0 level in the current calculation would explain the experimental EDMR observations. In this 0.5 eV window, only nitrogen-decorated defects would be spin active, because the neutral charge state of the silicon vacancy is known to be diamagnetic, and, hence, not observed in magnetic resonance. The Wang result [29] and Torpo result [27] would lead to little change, the spin-active state is already completely within the range of the SDCP experiment, and yielding no difference between the SDR and SDCP after the NO anneal.

Finally, we turn to the calculated spin densities, calculated from populations analysis, on the nitrogen ions. In Table II, we show the total spin densities on N-a, N-b, and N-c. We should note that these are pseudo-spin densities, obtained from the pseudo-wave functions. They do not include core-polarization, and they do not have the correct orthogonality oscillations that would permit direct calculation of hyperfine parameters. However, these sums over direction and a split-valence basis set are good first order approximations (to better than a factor of two) for estimates of broadening due to the hyperfine interactions with the nearby nitrogen atoms. Hyperfine constants for electrons 100% localized on the near 100% abundant ^{14}N sites [31, 32] allow for approximate calculation of the broadening. The isotropic hyperfine coupling constant for an electron 100% localized on a nitrogen s- orbital would be 646.2 Gauss. The anisotropic hyperfine coupling constant for an electron 100% localized on a nitrogen p- orbital would be 19.8 Gauss. Since the nitrogen nucleus has a spin of one and the s- contribution is somewhat larger than the p-

contribution, we estimate that the broadening would be dominated by the s- character contribution and would correspond to about 2.2 Gauss for nitrogen atoms at the N-a sites and 0.9 Gauss for nitrogen atoms at the N-b and N-c sites. The net effect would be a weighted average of these values. Thus the experimentally observed broadening of about 1.5 Gauss is in good agreement with the, admittedly, semi-quantitative theoretical values.

Summary

Our results provide a coherent explanation for the differences in the BAE/SDR and SDCP EDMR results for devices which have and have not been subjected to the technologically important NO anneals. Nitrogen atoms in close proximity to the silicon vacancy centers will both lower the –/0 energy levels and broaden the EDMR spectra. Our work is consistent with the earlier work of others indicating the presence of extremely high densities of nitrogen atoms at the SiC-oxide interface as a result of NO anneals [1,2]. It should be noted that our results also suggest that the NO anneals would be more effective in improving the performance of n-channel devices than p-channel devices as the introduction of the nitrogen atoms will drive remaining defect energy levels downward towards the interface SiC valence band edge.

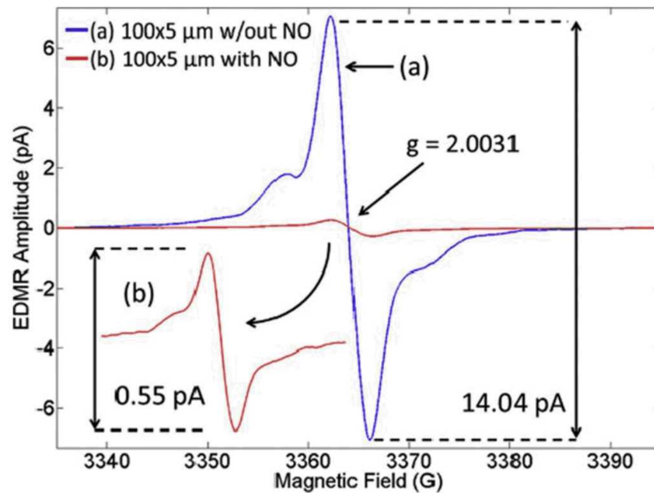

FIG. 1. The effects of an NO anneal on the SDCP detected EDMR. Two defect spectra are superimposed: a sharp center line, due to silicon vacancies in the near interface silicon carbide and a weaker spectrum, with two lines separated by about 11 G due to hydrogen complexed E′ centers. The NO anneal greatly reduces the amplitudes of both defect spectra [10].

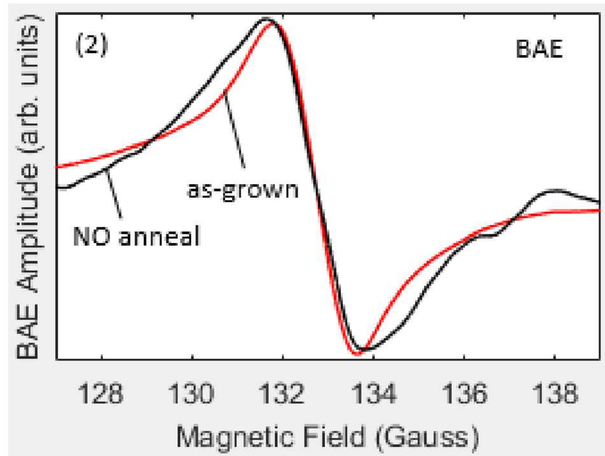

FIG. 2. 360 MHz BAE spectra comparing NO annealed (black) and as-grown (red) samples. Spectra are amplitude normalized for better comparison of linewidths.

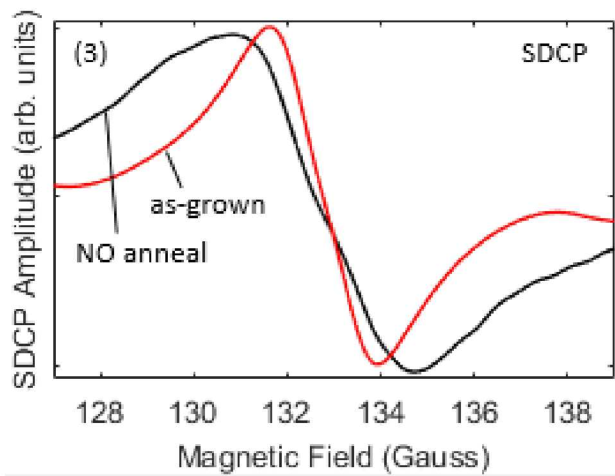

FIG. 3. 360 MHz SDCP spectra comparing NO annealed (black) and as-grown (red) samples. Spectra are amplitude normalized for better comparison of linewidths.

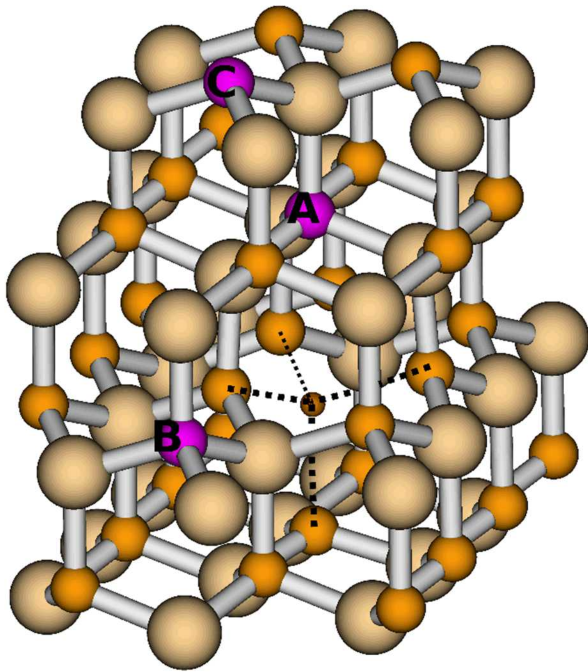

FIG. 4: Sites for nitrogen decoration (purple) in silicon carbide supercell Brown (tan) are carbon (silicon) atoms. Center of vacancy indicated by red atom. In all other figures and tables, A, B, and C will be referred to as N-a, N-b, and N-c.

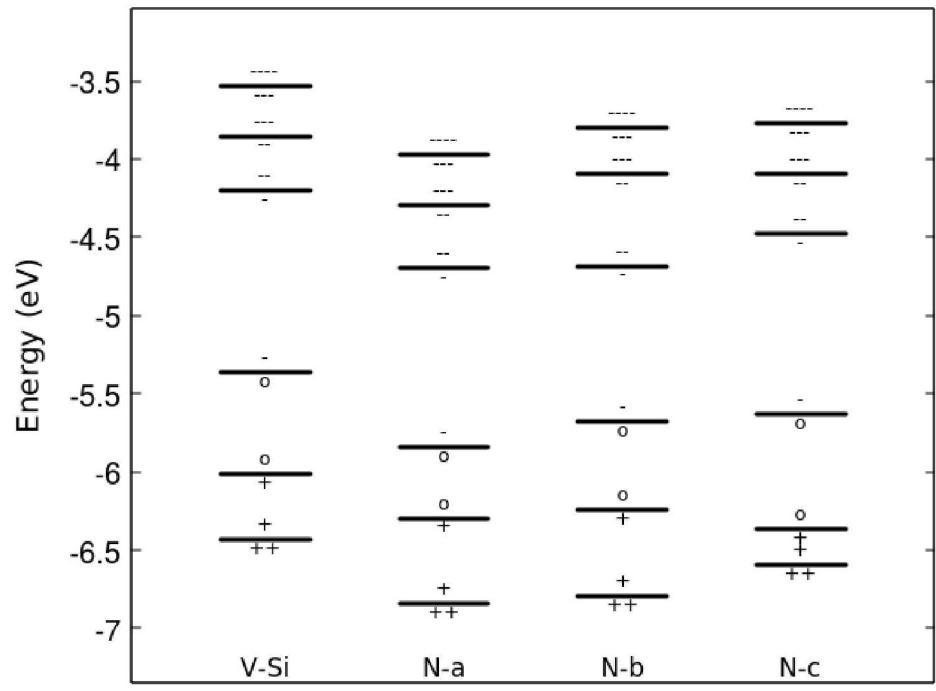

FIG. 5: Defect levels, as calculated using the LMCC, for the silicon vacancy, and for the three configurations in Fig. 4.

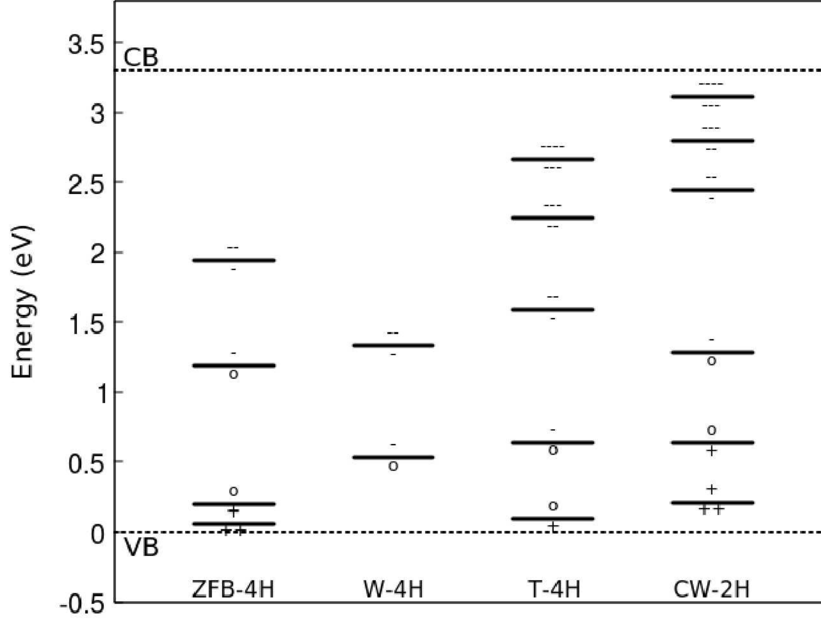

FIG. 6: Silicon vacancy defect levels from several calculations for 2H- and 4H-SiC. The band edges, estimated from the LMCC method, are shown in dotted lines. ZFB, W, T, and CW are from Ref. [28], [29], [27], and current work.

	$R_{N-V_{Si}}$ (Å)	ΔE_f (eV) (Si-Rich)
V_{Si}	-	2.75
N-a	3.36	4.94
N-b	4.78	4.96
N-c	5.87	5.11

TABLE I: Energies of formation and intra-defect distances for sites labeled in Fig. 4

	s-density	p-density	d-density
N-a	1.73e-3	2.46e-2	3.2e-4
N-b	7.0e-4	1.13e-2	6.4e-4
N-c	7.0e-4	1.12e-2	6.1e-4

TABLE II: Spin densities, in electron spins, on the three sites shown in Fig. 4.

Acknowledgements

AFRL gratefully acknowledge the support of the Air Force Office of Scientific Research through contract FA9550-17RVCOR505. This work was supported in part by a grant of computer time from the DoD High Performance Computing Modernization Program at the Air Force Research Laboratory and at the U. S. Army Engineer Research and Development Center. Work at Penn State was supported in part by AFOSR under grant # FA 9550-17-1-0242 and in part by the US Army Research Laboratory, Adelphi, MD. Sandia National Laboratories is a multi-mission laboratory managed and operated by National Technology and Engineering Solutions of Sandia, LLC., a wholly owned subsidiary of Honeywell International, Inc., for the U.S. Department of Energy's National Nuclear Security Administration under contract DE-NA0003525. This paper describes objective technical results and analysis. Any subjective views or opinions that might be expressed in the paper do not necessarily represent the views of the U.S. Department of Energy or the United States Government. AHE would like to thank Drs. Andrew C. Pineda and Danhong Huang for helpful questions and discussions. MAA and PML also thank Dr. Aivars J. Lelis of the US Army Research Laboratory, Adelphi, MD, for helpful discussions.

References

[1] R. Kosugi, T. Umeda, and Y. Sakuma, Appl. Phys. Lett. **99**, 182111 (2011).

[2] J. Rozen, S. Dhar, M. E. Zvanut, J. R. Williams, and L. C. Feldman, J. Appl. Phys. **105**, 124506 (2009).

[3] G. Y. Chung, C. C. Tin, J. R. Williams, K. McDonald, R. K. Chanana, R. A. Weller, S. T. Pantelides, L. C. Feldman, O. W. Holland, M. K. Das, and J. W. Palmour, IEEE Electron Dev. Lett. **22**, 176 (2001).

[4] G. Y. Chung, C. C. Tin, J. R. Williams, K. McDonald, M. Di Ventra, S. T. Pentelides, L. C. Feldman, and R. A. Weller, Appl. Phys. Lett. **76**, 1713 (2000).

[5] D. B. Habersat, A. J. Lelis, J. M. McGarrity, F. B. McLean, and S. Pothbare, Mater. Sci. Forum **600-603**, 743 (2009).

[6] T. Umeda, K. Esaki, R. Kosugi, K. Fukuda, T. Ohshima, N. Morishita, and J. Isoya, Appl. Phys. Lett. **99**, 142105 (2011).

[7] C. P. Slichter, Principles of Magnetic Resonance, Springer-Verlag Berlin Heidelberg (1990).

[8] D. J. Lepine, Phys. Rev. B **6**, 436 (1972).

[9] D. Kaplan, I. Solomon, and N. F. Mott, J. Phys. Lett. (Paris) **39**, 51 (1978).

[10] C. J. Cochrane, P. M. Lenahan, and A. J. Lelis, Appl. Phys. Lett. **102**, 193507 (2013).

[11] J. F. Conley and P. M. Lenahan, IEEE Trans. on Nucl. Sci. **40**, 1335 (1993).

[12] B. C. Bittel, P. M. Lenahan, J. T. Ryan, J. Fronheiser, and A. J. Lelis, Appl. Phys. Lett. **99**, 083504 (2011).

[13] T. Aichinger and P. M. Lenahan, Appl. Phys. Lett. **101**, 083504 (2012).

[14] J. S. Brugler and P. G. A. Jespers, IEEE Trans. Electron Dev. **ED-16**, 297 (1969).

[15] G. Groeseneken, H. E. Maes, N. Beltran, and R. F. De Keersmaecker, IEEE Trans. on Electron Dev. **ED-31**, 42 (1984).

[16] P. Heremans, J. Witters, G. Groeseneken, and H. E. Maes, IEEE Trans. on Electron Dev. **36**, 1318 (1989).

[17] D. R. Hamann, Phys. Rev. B **40**, 2980 (1989).

[18] J. P. Perdew, K. Burke, and M. Ernzerhof, Phys. Rev. Lett. **77**, 3865 (1996).

[19] P. A. Schultz, Phys. Rev. B **60**, 1551 (1999).

[20] P. A. Schultz, Phys. Rev. Lett. **84**, 1942 (2000).

[21] P. A. Schultz, Phys. Rev. Lett. **96**, 246401 (2006).

[22] P. A. Schultz and A. H. Edwards, Nucl. Instrum. & Methods B **327***,* 2 (2014).

[23] P. A. Schultz and O. A. von Lilienfeld, Modelling Simul. Mater. Sci. Eng. **17**, 084007 (2009).

[24] P. A. Schultz, J. Phys. Condens. Matter 27, 075801 (2015).

[25] R.M. Van Ginhoven and P.A. Schultz, J. Phys. Condens. Matter. **25**, 495504 (2013).

[26] W. Jost, J. Chem. Phys. **1**, 466 (1933).

[27] L. Torpo, M. Marlo, T. E. M. Staab, and R. M. Nieminen, J. Phys.: Condens. Matter **13**, 6203 (2001).

[28] A. Zywietz, J. Furthmüller, and F. Bechstedt, Phys. Rev. B **59**, 15166 (1998).

[29] X. Wang, M. Zhao, H. Bu, H. Zhang, X. He, and A. Wang, J. Appl. Phys. **114**, 194305 (2013).

[30] P. A. Schultz, R. Van Ginhoven, and A. H. Edwards, *unpublished*.

[31] J. A. Weil, J. R. Bolton, J. E. Wertz, Electron Paramagnetic Resonance , Elementary Theory and Practical Application, Wiley- Interscience, John Wiley and Sons, New York, (1994)

[32] J. R. Morton and K. F. Preston, J. Magnetic Resonance **30**, 577 (1978)